JOURNAL OF MATERIALS SCIENCE 21 (1986) 2185–2192

Crack healing and fracture strength of silicon crystals

K. YASUTAKE, M. IWATA*, K. YOSHII, M. UMENO, H. KAWABE
Department of Precision Engineering, Faculty of Engineering, Osaka University, 2-1 Yamada-Oka, Suita, Osaka 565, Japan

The influence of annealing at 700 to 1100° C on fracture strength of pre-cracked silicon wafers was examined by four-point bending tests at room temperature. The fracture strengths of the specimens annealed in oxygen increased significantly with increasing annealing temperature. On the other hand, annealing in vacuum showed little influence on the fracture strength. The strength increase by the annealing in oxygen was found to be caused by crack healing. Utilizing transmission electron microscopy, it is suggested that the crack surfaces were rebonded by the formation of a thin oxide layer at the crack interface. The activation energy for the crack healing was determined to be 2.0 ± 0.1 eV, which was consistent with that of the reaction-limited growth of thin oxide film.

1. Introduction

Dislocations in silicon single crystals and their plastic behaviour at elevated temperatures have been intensively studied in terms of dislocation dynamics or in relation to the wafer warpage in LSI manufacturing processes. On the other hand, the papers concerning the fracture characteristics of silicon crystals are rather scarce in spite of the fatal nature of cracking and brittle fracture in device processes. In recent years, backside damage is often induced in silicon wafers for impurity gettering purposes by means of sandblasting, abrasion or laser irradiation [1–5]. The damaged layer consists of dislocation networks and microcracks, arrangement of which varies with severity of the damage treatments [5, 6]. It is therefore desirable to acquire a fundamental understanding of the fracture characteristics of silicon wafers with microcracks particularly in the course of device fabrication processes.

Recently, some authors reported the fracture toughness or fracture surface energies of silicon [7–9]. Lawn *et al.* [10, 11] have studied the micromechanics of indentation-induced flaws, clarifying the role of residual contact stresses in the strength of the specimen. Utilizing the scanning electron microscope (SEM), Eggermont *et al.* [12] have studied laser-induced backside damage in the course of annealing processes and observed crack healing during a temperature cycle at 1050° C. However, crack healing processes and the influence of annealing atmospheres have not been studied in detail. In this work we studied the crack healing phenomenon of pre-cracked silicon wafers which were subjected to annealing under several kinds of atmosphere, and measured the strength of the wafers by four-point bending tests.

2. Experimental procedure

The commercial 100 mm diameter (0 0 1) silicon wafers from dislocation-free floating-zone (FZ) and Czochralski (CZ) ingots were utilized as specimens. Both types of crystals were doped with boron to a resistivity of 17 to 23 Ωcm. The concentration of interstitial oxygen atoms was determined by the infrared absorption method [13] to be about $8.5 \times 10^{17}\,cm^{-3}$ in CZ silicon wafers and below $1 \times 10^{16}\,cm^{-3}$ in FZ silicon wafers, respectively. The concentration of substitutional carbon atoms was less than the detection limit of infrared method in both types of wafer.

Samples for four-point bending fracture-tests were cut from these wafers along the ⟨1 1 0⟩ direction into the dimensions $0.5 \times 4 \times 32\,mm^3$, and then chemically polished to remove the surface damage with a solution of $CH_3COOH : HNO_3 : HF$ (1 : 10 : 1). As a precursor crack for the fracture test, a well-defined crack with a semi-elliptical form was produced by the Knoop diamond indentation method [8, 14, 15] at the centre of the tensile surface and in the {1 1 0} plane such that the crack was oriented perpendicular to the tensile stress. Fig. 1 illustrates the indentation on the tensile surface and the cross section of a Knoop-indented crack on the cleavage plane. Indentation load P was varied from 50 to 500 g to produce several sizes of cracks.

The cracked specimens were annealed in a quartz furnace at 700 to 1100° C in several kinds of atmosphere: flowing dry oxygen, flowing argon, vacuum of 2.6×10^{-4} Pa, or air. The four-point bending tests were conducted at room temperature with a crosshead displacement rate of $0.02\,mm\,min^{-1}$ using stainless-steel load-supports attached to Instron universal testing machine (TTCM-L). Distances between the two

Present address: Mizuno corporation, Fukushima-Ku, Osaka 553, Japan.

0022–2461/86 $03.00 + .12 © *1986 Chapman and Hall Ltd.*

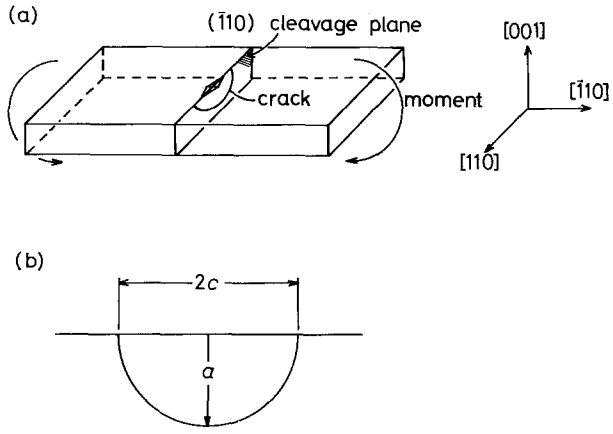

Figure 1 (a) Schematic diagram of bending specimen with Knoop indentation on tensile surface, and (b) cross section of Knoop-indented crack.

lower supports and between the upper supports were 25 and 10 mm, respectively. The fracture tensile stress, σ_f, at the outermost surface was calculated by the simple elastic beam theory [16].

Fractographic observations were made on the fracture surfaces utilizing SEM. Some samples with healed cracks were observed by transmission electron microscopy (TEM) HU-3000 operated at 2000 kV. The method of specimen preparation for TEM was similar to that in the work by Hockey and Lawn [17]. Auger electron microanalysis was carried out on one of the partially healed cracks utilizing scanning Auger microprobe (JAMP-10) operated at 10 keV with a beam diameter of 1 μm.

3. Results

3.1. Fracture strength after annealing in vacuum

A rather large crack with a depth of about 50 μm was induced in the specimen (with P = 500 g), and the fracture stress, σ_f of the pre-cracked specimen was measured at room temperature after annealing the specimen in vacuum. Figs 2a and b show σ_f as a function of annealing temperature for isochronal annealings of 2 and 20 h, respectively. Each point represents an average of five test results with an error bar indicating upper and lower limits of data. Since no meaningful difference is seen between FZ and CZ wafers, dissolved oxygen atoms in silicon have a negligible effect on cracks in the present experiments. σ_f of the annealed wafers is slightly larger than that of the as-indented wafers, but is independent of the annealing temperature for both isochronal annealings. The slight increase of σ_f is considered to be caused by the relaxation of indentation-induced residual stress which acts as a driving force for crack extension [11].

At the fracture stress all the specimens broke into two pieces by the extension of the precursor cracks. Scanning electron microscopy of fracture surfaces revealed the crack profile as shown in Fig. 3. A small amount of stable crack growth before catastrophic propagation to fracture is seen on the as-indented specimen (Fig. 3a) presumably due to the presence of the indentation-induced residual stress field [11]. On annealing at 700° C for 2 h in vacuum, the crack remains semi-elliptical but the stable crack growth is not observed in this case (Fig. 3b) where the annealing

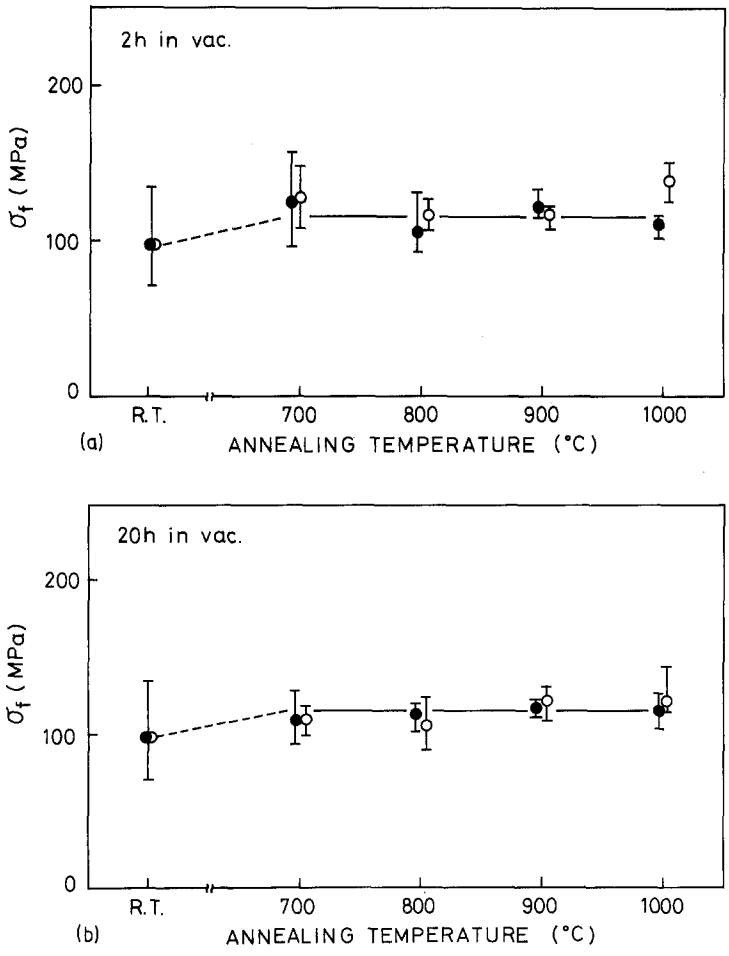

Figure 2 Effect of annealing in vacuum on fracture stress, σ_f, of pre-cracked FZ and CZ silicon specimens. (Knoop indentation with load P = 500 g.) (a) 2 h isochronal annealing, and (b) 20 h isochronal annealing. (●) FZ, (○) CZ.

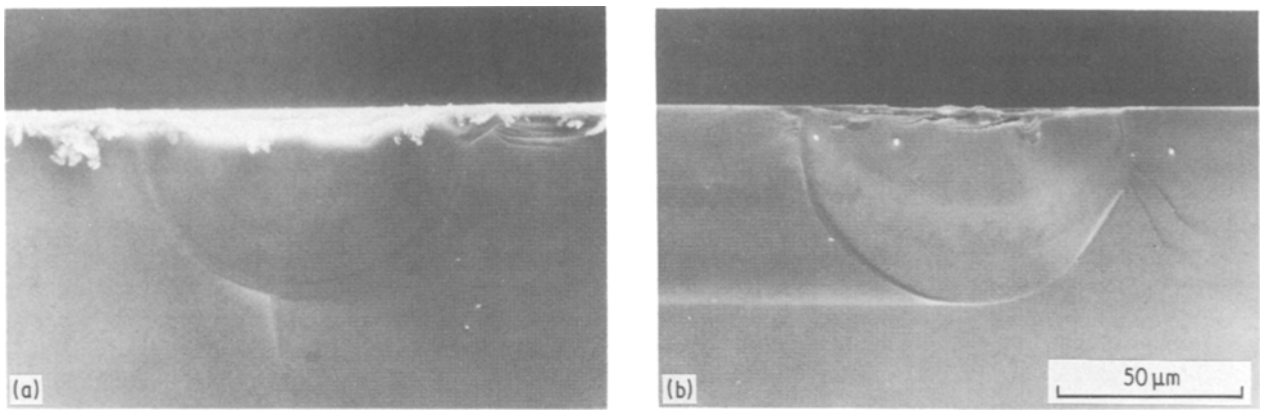

Figure 3 Scanning electron micrographs showing profiles of 500 g Knoop-indented cracks observed on fracture surfaces of FZ silicon specimens. (a) As-indented specimen, (b) fractured after annealing at 700° C for 2 h in vacuum.

has caused the relaxation of the residual stress. After the annealings at other temperatures in vacuum the cracks had almost the same shape and size as that in Fig. 3b, which is consistent with the independence of σ_f on annealing temperature (Fig. 2).

3.2. Fracture toughness of silicon

The residual stress around the indentation mark was released by the annealings in vacuum, and the crack profile of the annealed specimens was similar to that of the as-indented ones as described in Section 3.1. Therefore, the vacuum-annealed specimens with precursor cracks can be used for the determination of fracture toughness values of silicon crystals. Measuring the depth of the crack a and σ_f of the specimen, we can calculate the fracture toughness K_{Ic} (critical stress intensity factor) on the fracture plane, according to the formula

$$K_{Ic} = \sigma_f M_b (\pi a/Q)^{1/2} \quad (1)$$

for a semi-elliptical surface crack in bending. Here, M_b is the elastic stress intensity magnification factor and Q is the flaw shape parameter. Details of these parameters for brittle materials have been described by several authors [14, 15, 18].

SEM observation of the fracture surfaces showed that the fracture initiated on the {1 1 0} plane, but as the crack propagated across the sample the fracture plane shifted to the {1 1 1} plane. The observed fracture patterns closely resembled that found by Chen and Leipold [8].

According to Equation 1, σ_f is plotted as a function of the inverse square root of the initial crack depth in Fig. 4. For the specimens annealed at 700° C for 2 h in vacuum, a linear relation is obtained between σ_f and $a^{-1/2}$. Data for the as-indented specimens show the same relation as the annealed ones in the smaller $a^{-1/2}$ region than about 0.15 $\mu m^{-1/2}$. In the larger region of $a^{-1/2}$, however, data for the as-indented specimens become lower than the line of the annealed ones. This means that K_{Ic} of the as-indented specimens appears smaller than that of the annealed ones and depends on the indentation load P, when P is smaller than around 400 g. The indentation load dependence of K_{Ic} of as-indented specimens has also been observed by Chen and Leipold [8]. The residual stress around the indentation mark is considered to lower the strength of the wafers and cause the indentation load dependence of K_{Ic}.

A probable value of K_{Ic} at room temperature was obtained from the line in Fig. 4 (with a standard deviation) to be

$$K_{Ic} = 0.91 \pm 0.09\,\text{MPa m}^{1/2} \ (\{1\,1\,0\} \text{ orientation}). \quad (2)$$

By the similar method, K_{Ic} for {1 0 0} orientation was obtained to be

$$K_{Ic} = 0.95 \pm 0.10\,\text{MPa m}^{1/2} \ (\{1\,0\,0\} \text{ orientation}). \quad (3)$$

These values are close to those obtained by Chen and

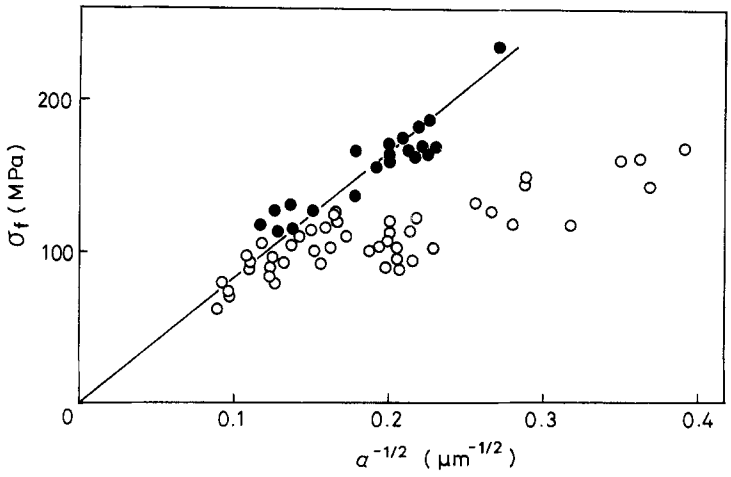

Figure 4 Plot of fracture stress, σ_f against (crack depth)$^{-1/2}$, $a^{-1/2}$ for (○) as-indented and (●) vacuum-annealed FZ silicon specimens (700° C for 2 h).

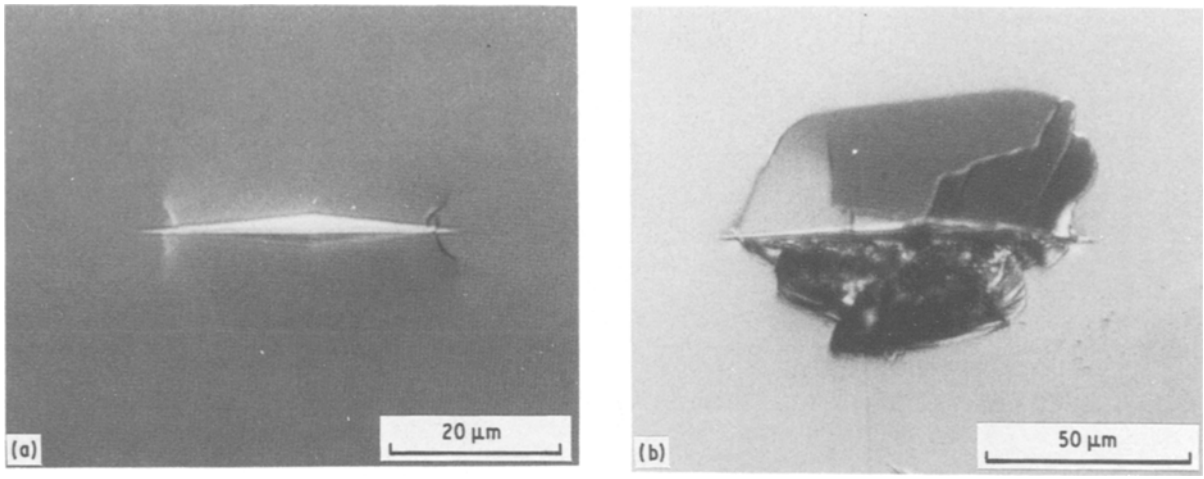

Figure 5 Optical micrographs of Knoop indentation marks on (0 0 1) surface. (a) $P = 100$ g; (b) $P = 500$ g.

Leipold using $P = 500$ g [8]. When P is larger than about 400 g, it is considered that the residual stress is released by the chipping of the indentation mark as a result of extension of lateral cracks.

Fig. 5 shows optical micrographs of indentation marks observed on the specimen surface for $P = 100$ and 500 g. In these photographs, median–radial cracks give little contrast and are hardly observed. It can be noticed that lateral crack extension and chipping of the material around the indentation mark are significant for $P = 500$ g. The lower half of the chip with the indentation mark is missing in Fig. 5b. The depth of the crater produced by surface chipping with $P = 500$ g is approximately 5 μm, which is deeper than the depth of the indentation mark (about 3 μm).

3.3. Fracture strength after annealings in oxygen and crack healing

In contrast to the vacuum annealings, the annealings in oxygen atmosphere significantly increased the fracture strength of pre-cracked specimens ($P = 500$ g). Fig. 6 shows σ_f after 2 h of isochronal annealings as a function of temperature. σ_f increases with increasing annealing temperature and σ_f after the annealing at 1000° C for 2 h is about 2.6 times as large as that after the vacuum annealings (Fig. 2).

By annealing at 1000° C for 2 h in oxygen, an oxide layer about 0.15 μm thick was produced on the specimen surface. In order to study the influence of the oxide layer on σ_f, the surface oxide layer was removed by ultrasonic agitation in a solution of HF(46%) : H_2O (1 : 20) for 15 or 60 min. Before the HF treatment, the measured σ_f is in the range 270 to 420 MPa, and after the treatment 240 to 410 MPa. This result indicates that the surface oxide layer has negligible effect on the fracture strength of silicon wafers. Thus, the fracture tests were carried out on the annealed specimens without removal of the oxide layer.

Annealing time dependences of σ_f are depicted in Fig. 7 for various annealing temperatures. At each temperature, σ_f increases with annealing time and approaches the stress level which corresponds to the average strength of the as-received specimens without precursor cracks. Fractographic observations revealed that the cracks after the annealings in oxygen are much smaller than those of as-indented and vacuum-annealed wafers as shown in Figs 3 and 8. Consequently, it can be concluded that the strength increment by the oxygen annealing is attributed to the crack healing. In the specimen annealed at 1000° C for 2 h in oxygen, one cannot see a trace of the precursor crack, and the fracture initiated at the crater produced by the extension of lateral cracks. This situation is more clearly seen in a plan-view of the specimen in Fig. 9. The entire indentation mark remains because the fracture initiated at a site other than the median–radial crack. It should be mentioned that all the tested

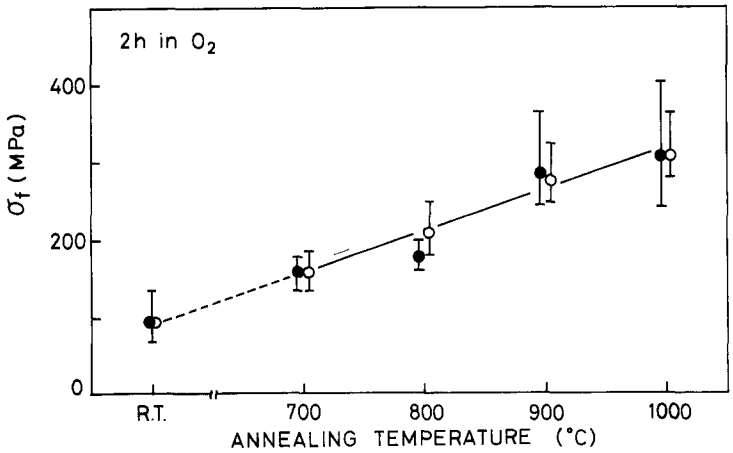

Figure 6 Effect of annealing in oxygen on fracture stress σ_f of pre-cracked FZ and CZ silicon specimens ($P = 500$ g). 2 h isochronal annealing. (●) FZ, (○) CZ.

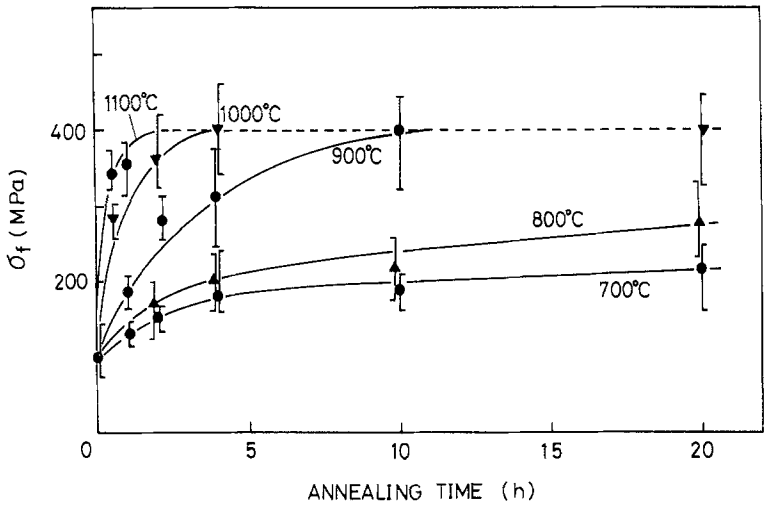

Figure 7 Increase of fracture stress σ_f of pre-cracked FZ silicon specimens by annealing in oxygen at various temperatures (P = 500 g).

specimens which were annealed at 1000° C for 2 h in oxygen fractured at a site other than the median–radial crack.

Here are described briefly the effects of the other annealing atmospheres. No crack healing was observed by the annealing at 800° C in argon atmosphere similar to the vacuum annealings. By annealing in air, however, the cracks were healed completely at 700° C for 50 min, which is much shorter than the required time for the complete healing in oxygen. Water vapour or some unintentional impurities in the air might promote crack healing, but the responsible cause is not known at present.

3.4. TEM observation of healed cracks

Hockey and Lawn [17] and Wiederhorn *et al.* [19] observed the microstructure of healed cracks in Al_2O_3 by TEM and revealed that the healed portion consisted of dislocation networks and voids originating from rebonding between matrix materials. Recently, Eggermont *et al.* [12] reported that laser irradiation-induced microcracks in silicon wafers were healed by annealings at 1050° C. They observed dislocation etch pits on the cleaved surface where microcracks should have existed before the annealing and attributed them to the healed configuration of microcracks similar to the TEM observation by Hockey and co-workers [17, 19].

In order to investigate the microstructure of healed cracks, we performed TEM observations of cracks which were healed completely by annealing at 1000° C for 2 h in oxygen. The observed portion was the median–radial crack front located near the intersection of the crack with the indented surface because the maximum K_I was expected to occur at this site upon bending tests [18, 20]. Most of the cracks were

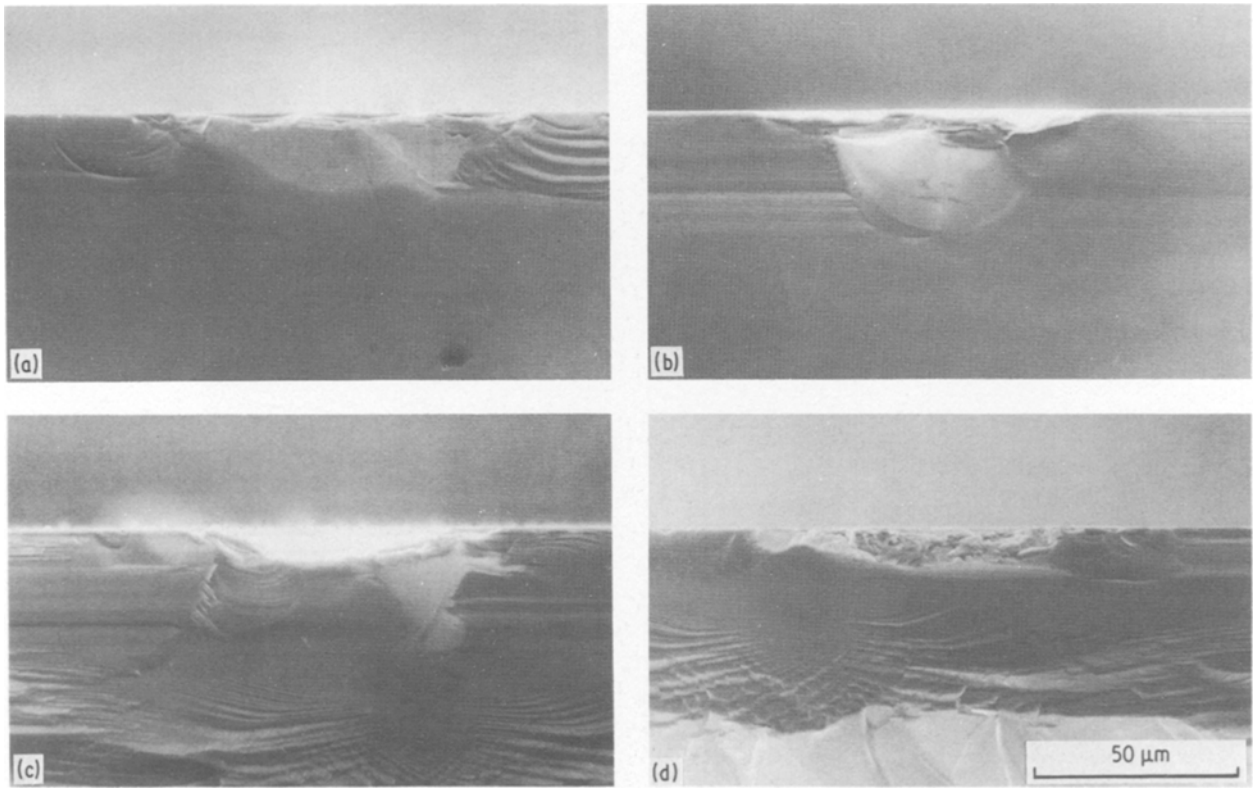

Figure 8 Fracture surfaces of pre-cracked FZ silicon specimens (P = 500 g) after annealing in oxygen. (a) 700° C, 2h; (b) 800° C, 2 h; (c) 900° C, 2 h; (d) 1000° C, 2 h.

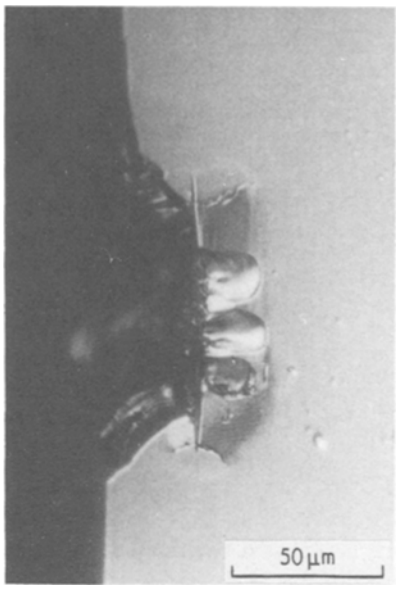

Figure 9 Plan view of the fractured specimen after the same experiment as that of Fig. 8d. Fracture initiated at a site other than the indentation induced median–radial crack.

observed as narrow bands because the crack interface was normal to the foil surface. In some cases, the crack interface deviated slightly from the {1 1 0} plane and the interfacial images were observed clearly. Fig. 10 shows TEM images of the median–radial crack front observed under the different diffraction vectors $\boldsymbol{g}$. In this case the crack interface is exactly on the {1 1 0} plane in the upper part of the photographs but it deviates slightly from the {1 1 0} plane near the crack front. We cannot see dislocation networks or voids at the crack interface in Fig. 10, and this was the same with other cracks on exact {1 1 0} plane. The interfacial images consist of Moiré type fringe patterns which vary with $\boldsymbol{g}$ [21] overlapped with thickness extinction fringes.

The Moiré fringe system is generated when the overlapping crystal portions have a small mismatch in lattice spacings or orientation such that there is a small difference in diffraction vector.

$$\Delta \boldsymbol{g} = \boldsymbol{g}_1 - \boldsymbol{g}_2 \neq 0 \tag{4}$$

The Moiré fringe patterns appear perpendicular to $\Delta \boldsymbol{g}$

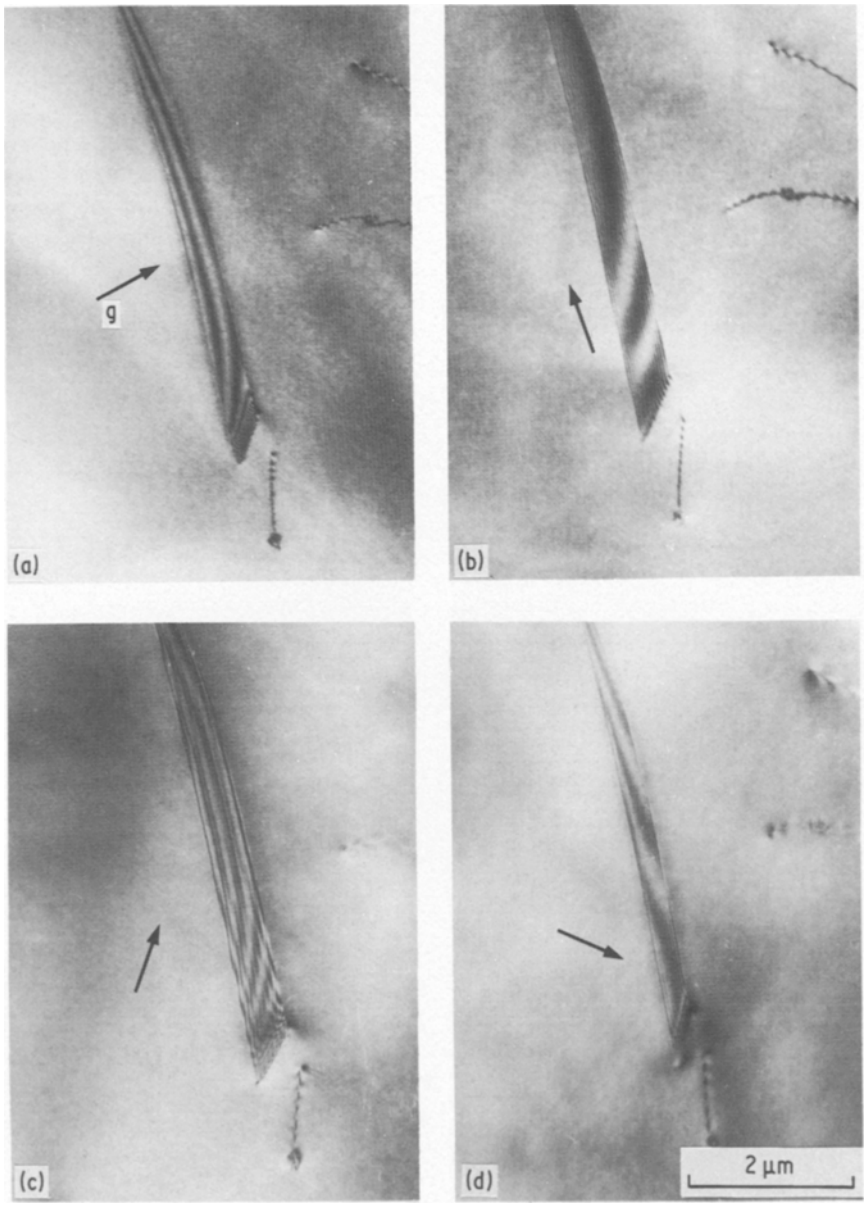

Figure 10 Transmission electron micrographs of a completely healed median–radial crack under different diffraction vectors $\boldsymbol{g}$. (a) $\boldsymbol{g} = 2\bar{2}0$, (b) $\boldsymbol{g} = 220$, (c) $\boldsymbol{g} = 400$, (d) $\boldsymbol{g} = 0\bar{4}0$. The pre-cracked specimen ($P = 50$ g) was annealed at 1000° C for 2 h in oxygen.

[21–23]. As the lattice spacings on both sides of the crack interface are considered to be the same, the Moiré fringes at the crack interface can be assumed to be of rotation Moiré type. The Moiré fringe directions seen in Fig. 10 deviate significantly from the direction of $\boldsymbol{g}$, except the upper right part of Fig. 10b where the intersection of the crack and the surface is parallel to $\boldsymbol{g}$. According to Gevers *et al.* [23], these geometrical aspects indicate that the rotation axis is not normal to the foil surface and that its lateral component in the foil surface is not parallel to $\boldsymbol{g}$. Therefore, the residual displacement field is complex and cannot be described by a simple displacement mode. More rigorous observations are necessary to draw any quantitative conclusion about the residual displacement field.

The interfacial images seen in Fig. 10 are similar to those observed for non-healed cracks in silicon [24], SiC [17, 24] or Al_2O_3 [17, 19, 24]. Consequently, it can be concluded that the crack healing is not caused by the rebonding of Si–Si atoms. It seems natural to think that there exists a thin layer of silicon oxide in the healed crack interface. The existence of silicon oxide phase in the interface was confirmed by the scanning Auger electron microanalysis. We analysed the partially healed crack (Fig. 8c) on the fracture surface. After sputtering some surface adsorption layer, a chemically shifted silicon peak at 78 eV corresponding to the silicon oxide phase was observed at the healed part. However, only a 91 eV peak corresponding to bare silicon was observed at the fracture surface other than the initial crack.

In Fig. 10a a slight contrast is seen along the traces of the intersection of the crack interface and the specimen surfaces, which is invisible when $\boldsymbol{g}$ is set almost parallel to the traces (Fig. 10b). This may indicate that the interfacial thin oxide layer induces a compressive stress component perpendicular to the interface owing to the volume expansion of the silicon oxide.

4. Discussion

We observe that the cracks in silicon crystals were healed by the annealings in the atmosphere containing oxygen. In the literature, the rate-limiting processes for the thermal crack healing were said to be the diffusion process in some oxide crystals [25–28] or the surface oxidation in SiC [29]. In the case of silicon, the oxidation process is clearly concerned with the crack healing mechanism. Therefore, we estimate the activation energy of crack healing and compare it with that for oxidation of silicon. The activation energy for the crack healing was determined from the σ_f against annealing time curves at several temperatures shown in Fig. 7 utilizing the cross-cut method described elsewhere [30].

Fig. 11 shows the equivalent time which is required for the specimens to gain the σ_f of 250 and 350 MPa as a function of reciprocal temperature. A single activation process operated in the temperature range 700 to 1100° C. The slope of the lines in Fig. 11 gives the activation energy of 2.0 ± 0.1 eV. The reported activation energy of oxidation process of silicon is 1.2 eV for the diffusion-limited growth of thick oxide films

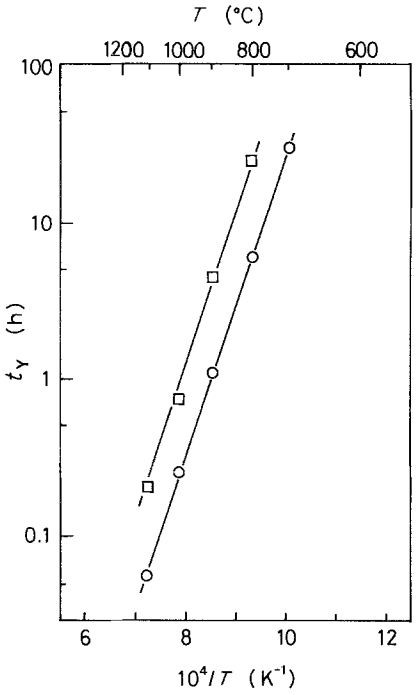

Figure 11 Equivalent times, t_Y, and temperatures characterizing particular states of crack healing obtained from the cross cuts of the curves in Fig. 7 with σ_f = (○) 250 and (□) 350 MPa.

and 2.0 eV for the reaction-limited growth of thin oxide films, respectively [31–33]. The activation energy of crack healing in silicon observed in this study is consistent with that of the reaction-limited growth of thin oxide film.

In conclusion, we can describe the crack healing process in silicon as follows. Initially the residual stress around the indentation mark is released and the crack surfaces become close together at elevated temperatures. The crack surfaces are rebonded by the formation of a thin layer of SiO_2 phase, the process of which is considered to begin from a crack front and then spread to the entire part of the crack. The rate limiting process is the reaction of silicon and oxygen atoms at the crack surface. As the Si–O bonding is stronger than Si–Si bonding [34], specimens break at the site other than the healed crack site upon fracture tests.

Acknowledgements

The authors thank Professor H. Fujita, Messrs K. Yoshida, M. Komatsu and T. Sakata of Osaka University for their kind cooperation in the use of HVEM HU-3000, and also Professor M. Uemura of Toyohashi University of Technology for permission and cooperation in the use of scanning Auger microprobe (JAMP-10). They are also indebted to Messrs S. Kawazu and J. Mitsuhashi of Mitsubishi Electric Corporation for supplying silicon wafers.

References

1. E. J. METS, *J. Electrochem. Soc.* **112** (1965) 420.
2. D. POMERANTZ, *J. Appl. Phys.* **38** (1967) 5020.
3. C. L. REED and K. M. MAR, *J. Electrochem. Soc.* **127** (1980) 2058.
4. Y. HAYAFUJI, T. YANADA and Y. AOKI, *ibid.* **128** (1981) 1975.
5. G. E. J. EGGERMONT, D. F. ALLISON, S. A. GEE,

K. N. RITZ, R. J. FALSTER and J. F. GIBBONS, in "Laser and Electron Beam Interaction with Solids", edited by B. R. Appleton and G. K. Celler (North-Holland, New York, 1982) p. 615.
6. R. STICKLER and G. R. BOOKER, *Phil. Mag.* **8** (1963) 859.
7. C. ST. JOHN, *ibid.* **32** (1975) 1193.
8. C. P. CHEN and M. H. LEIPOLD, *Amer. Ceram. Soc. Bull.* **59** (1980) 469.
9. C. MESSMER and J. C. BILELLO, *J. Appl. Phys.* **52** (1981) 4623.
10. B. R. LAWN, A. G. EVANS and D. B. MARSHALL, *J. Amer. Ceram. Soc.* **63** (1980) 574.
11. B. R. LAWN, D. B. MARSHALL and P. CHANTIKUL, *J. Mater. Sci.* **16** (1981) 1769.
12. G. E. J. EGGERMONT, S. A. GEE, C. G. M. van KESSEL, R. J. FALSTER and J. F. GIBBONS, *Appl. Phys. Lett.* **41** (1982) 1133.
13. W. KAISER and P. H. KECK, *J. Appl. Phys.* **28** (1957) 882.
14. J. J. PETROVIC, L. A. JACOBSON, P. K. TALTY and A. K. VASUDEVAN, *J. Amer. Ceram. Soc.* **58** (1975) 113.
15. J. J. PETROVIC and L. A. JACOBSON, *ibid.* **59** (1976) 34.
16. S. P. TIMOSHENKO and J. N. GOODIER, "Theory of Elasticity" (McGraw Hill, New York, 1951).
17. B. J. HOCKEY and B. R. LAWN, *J. Mater. Sci.* **10** (1975) 1275.
18. R. H. KEAYS, Structure and Materials Rept. 343, Department of Supply, Australian Defence Scientific Service, Aeronautical Research Laboratories, April (1973).
19. S. M. WIEDERHORN, B. J. HOCKEY and D. E. ROBERTS, *Phil. Mag.* **28** (1973) 783.
20. F. W. SMITH, A. F. EMERY and A. S. KOBAYASHI, *J. Appl. Mech.* **34** (1967) 953.
21. P. B. HIRSCH, A. HOWIE, R. B. NICHOLSON, D. W. PASHLEY and M. J. WHELAN, "Electron Microscopy of Thin Crystals" (Plenum, New York, 1965).
22. R. GEVERS, *Phil. Mag.* **7** (1962) 1681.
23. R. GEVERS, J. VAN LANDUYT and S. AMELINCKX, *Phys. Status Solidi* **18** (1966) 325.
24. B. R. LAWN, B. J. HOCKEY and S. M. WIEDERHORN, *J. Mater. Sci.* **15** (1980) 1207.
25. C. F. YEN and R. L. COBLE, *J. Amer. Ceram. Soc.* **55** (1972) 507.
26. A. G. EVANS and E. A. CHARLES, *Acta Metall.* **25** (1977) 919.
27. J. T. A. ROBERTS and B. J. WRONA, *J. Amer. Ceram. Soc.* **56** (1973) 297.
28. G. BANDYOPADHYAY and J. T. A. ROBERTS, *ibid.* **59** (1976) 415.
29. F. F. LANGE, *ibid.* **53** (1970) 290.
30. J. BURKE, "The Kinetics of Phase Transformation in Metals" (Pergamon, London, 1965).
31. B. E. DEAL and A. S. GROVE, *J. Appl. Phys.* **36** (1965) 3770.
32. D. W. HESS and B. E. DEAL, *J. Electrochem. Soc.* **124** (1977) 735.
33. B. E. DEAL, *ibid.* **125** (1978) 576.
34. L. PAULING, "The Nature of the Chemical Bond" (Cornell University Press, New York, 1960).

Received 17 June
and accepted 10 September 1985